5G Multi-User System Simulations in Line-of-Sight With Space-Tapered Cellular Base Station Phased Arrays

Aslan, Yanki; Salman, Salman; Puskely, Jan; Roederer, Antoine; Yarovoy, Alexander

Publication date
2019

Document Version
Final published version

Published in
2019 13th European Conference on Antennas and Propagation (EuCAP)

5G Multi-User System Simulations in Line-of-Sight With Space-Tapered Cellular Base Station Phased Arrays

Yanki Aslan[1], Salman Salman[2], Jan Puskely[3], Antoine Roederer[4], Alexander Yarovoy[5]
MS3 Group, Department of Microelectronics, Faculty of EEMCS
Delft University of Technology, The Netherlands
{[1]Y.Aslan, [3]J.Puskely-1, [4]A.G.Roederer, [5]A.Yarovoy}@tudelft.nl, [2]Salman@student.tudelft.nl

***Abstract*—The performance of space-tapered multi-beam arrays with minimized side lobe levels is statistically evaluated in a line-of-sight propagation environment within a cell sector in terms of the signal-to-interference-plus-noise ratio at the multiple user ends. Comparative analyses are performed to examine the advantages of space-tapered, irregular arrays over the conventional regular array layouts. The system model is formulated with a meaningful link-budget analysis. Two different precoding techniques, conjugate beamforming and zero-forcing, are applied to compute the excitation coefficients at the antenna elements. The effects of several practical factors such as approaches in user scheduling, errors in channel state information estimation and quantization in excitation amplitudes and phases are studied. The simulation results indicate that space-tapered arrays with conjugate beamforming statistically perform better than the regular counterparts and can achieve similar performance to zero-forcing precoding when the impact of non-ideal system conditions is considered.**

***Index Terms*—aperiodic array, conjugate beamforming, fifth generation (5G) base station, multi-user communication, space tapering, zero-forcing.**

I. Introduction

Future 5G cellular networks are expected to provide multi-gigabit-per-second data rates with low latencies in various application scenarios that have different requirements on the base station antennas in terms of the gain, number of beams, side lobe levels and positions, beamwidths, scan ranges and so on. In order to maximize the data-rate performance of the system, antenna design methodologies in 5G should focus on the specific use case and the propagation environment. Therefore, embedding the channel model and propagation aspects in the antenna design has gained a lot of interest in 5G systems, especially in the past few years [1]–[3].

In this paper, statistical performance of the space-division-multiple-access (SDMA) beamforming is studied in a multi-user random LoS downlink mobile communication environment, based on regular and irregular (space-tapered) array layouts. Space-tapered arrays are particularly interesting for 5G applications due to their optimum power efficiency and relatively low side lobe levels [4], [5]. The performance of the layouts are evaluated in terms of the SINR at the users for two well-known linear precoding techniques [6]: conjugate beamforming (CB) and zero-forcing (ZF).

Exploiting layout irregularity in SDMA has been recently introduced in the antenna design community and showed good potential in increasing the channel capacity [7], [8]. Although there are previous studies on the system performance evaluation of irregular arrays, to our knowledge, study of different precoding techniques with a meaningful link budget analysis has not been performed. The novelty of our work lies in the inclusion of the link-budget analysis considering such parameters as EIRP, base station height, user positions, cell range, sector width, thermal noise etc., together with the commonly used precoding algorithms. Effect of many practical factors regarding user scheduling, channel state information (CSI) and excitation quantization are also studied.

It is worthy of note that SDMA applied here can be realized by fully-digital [9] or hybrid (fully-connected [10] or partially-connected [11]) architectures. Due to high complexity and cost of fully-digital systems, hybrid architectures with less number of RF chains (N_{RF}) are currently used in the industry. Between the two hybrid beamforming architectures proposed in the literature, the fully-connected structure can provide more (simultaneous) beams with larger gains, as compared to the partially-connected one with the same number of antenna elements. This performance improvement in the fully-connected approach comes at the expense of having larger power amplifiers that compensate the combining loss (which, for example, is equal to 6 dB for N_{RF} = 4).

The paper is organized as follows. Section II presents the system model and formulation. The simulation results are provided and discussed in Section III. Section IV concludes the paper.

II. System Model

A. Model Formulation

Consider a single cell SDMA system with narrowband carriers where a base station (BS) is equipped with M antenna elements, serving K single antenna users simultaneously in the same frequency band. Let the vector $\boldsymbol{q}$ denote the symbol intended for the users with $E\{|q_k|^2\} = 1$, $\boldsymbol{\rho}$ is the vector containing the SNR at the users, vector $\boldsymbol{n}$ contains the unit variance Additive White Gaussian Noise (AWGN) at each user and $\boldsymbol{y}$ is the vector containing the received user signals.

$$\boldsymbol{q} \in \mathbb{C}^{Kx1}, \quad \boldsymbol{\rho} \in \mathbb{R}^{Kx1}, \quad \boldsymbol{n} \in \mathbb{C}^{Kx1}, \quad \boldsymbol{y} \in \mathbb{C}^{Kx1} \tag{1}$$

The linearly precoded signal vector $\boldsymbol{x}$ is given by

$$\boldsymbol{x} = \boldsymbol{W}\boldsymbol{q} \tag{2}$$

where $\boldsymbol{W}$ is the precoding matrix.

$$\boldsymbol{W} \in \mathbb{C}^{MxK} \;\; s.t. \;\; \sum_{m=1}^{M} |W_{m,k}|^2 = 1 \;\; \text{for} \;\; \forall k \in \{1, \ldots, K\} \tag{3}$$

Let $\boldsymbol{H}$ denote the downlink channel matrix with normalized entries such that

$$\boldsymbol{H} \in \mathbb{C}^{KxM} \quad s.t. \quad E\{|H_{k,m}|^2\} = 1 \tag{4}$$

Then, the received signal vector at the users is given by

$$\boldsymbol{y} = \boldsymbol{\rho} \cdot (\boldsymbol{H}\boldsymbol{x}) + \boldsymbol{n} \tag{5}$$

In a random LoS channel, the channel between the receive antenna at the k-th user (with position $\boldsymbol{r}_k$) and the m-th transmit antenna element at the base station (with position $\boldsymbol{r}_m$) can be formulated as [12]

$$H_{k,m} = \beta_{k,m} G_m(\hat{\boldsymbol{r}}_{km}) G_k(-\hat{\boldsymbol{r}}_{km}) \frac{e^{-j\frac{2\pi}{\lambda}|\boldsymbol{r}_k - \boldsymbol{r}_m|}}{|\boldsymbol{r}_k - \boldsymbol{r}_m|} \tag{6}$$

where $G_m(\hat{\boldsymbol{r}}_{km})$ and $G_k(-\hat{\boldsymbol{r}}_{km})$ are the far-field functions of the transmit and receive elements, respectively, in the corresponding direction $\hat{\boldsymbol{r}}_{km}$. For single omni-directional antenna users, $G_k(-\hat{\boldsymbol{r}}_{km})$ is equal to 1. $\beta_{k,m}$ is the normalization constant satisfying (4). The SINR of the transmission from the BS array to the k-th single antenna user is given by

$$SINR_k = \frac{\rho_{k,k} |\boldsymbol{H}_{k,:} \boldsymbol{W}_{:,k}|^2}{\sum_{j \neq k}^{K} \rho_{k,j} |\boldsymbol{H}_{k,:} \boldsymbol{W}_{:,j}|^2 + 1} \tag{7}$$

where numerator indicates the received signal power and denominator indicates the received interference plus noise power (note that the terms are normalized with respect to the noise power). $\rho_{k,j}$ is the SNR computed at the k-th user while serving the j-th user, which is given by

$$\begin{aligned} \rho_{k,j}(dB) = P_j(dBm) - 20\log_{10}[f_c] - 20\log_{10}[\frac{4\pi}{c}] \\ - 20\log_{10}[|\boldsymbol{r}_k - \boldsymbol{r}_m|] + G_m(\hat{\boldsymbol{r}}_{km})(dB) \\ + G_k(-\hat{\boldsymbol{r}}_{km})(dB) - P_{th}(dBm) \end{aligned} \tag{8}$$

where f_c is the carrier frequency, P_j is the average transmit power of the j-th user and P_{th} is the thermal noise power (see Table I for the chosen values). The precoding matrix (or the antenna excitation weights) $\boldsymbol{W}$ is computed according to the selected method, namely the conjugate beamforming (CB) which maximizes the power towards the users or zero-forcing (ZF) which minimizes the interference among the users [6].

$$\boldsymbol{W} = \begin{cases} \boldsymbol{H}^{\dagger} & for\ CB \\ \boldsymbol{H}^{\dagger}(\boldsymbol{H}\boldsymbol{H}^{\dagger})^{-1} & for\ ZF \end{cases} \tag{9}$$

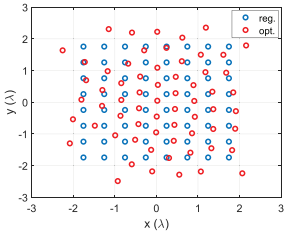

Fig. 1. Element locations of the regular and space-tapered array (obtained using [5]).

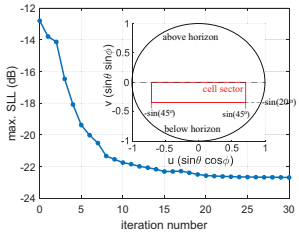

Fig. 2. Definition of the cell sector in the uv-plane and convergence of the max. SLL obtained using [5].

where the symbol † denotes the Hermitian transpose.

The signal processing in CB is very simple and more robust to channel impurities as compared to the ZF which relies on the pseudo-inverse of the channel matrix. Therefore, achieving close performance to ZF by CB using smart antenna layouts is very important to reduce the complexity and computational burden on the mm-wave 5G systems [13].

B. Simulation Scenario

We assume a sector antenna with M = 64 patch antenna elements in a regular and irregular layout with adjustable amplitudes and phases for each of the K = 4 users. The regular layout is an 8x8 half-wavelength spaced array while the irregular one is the optimized space-tapered array using the method [5], which minimizes the maximum side lobe level (SLL) when the beam is scanned inside the sector defined by a 20 degree range in user elevation below horizon and a 90 degree range in user azimuth. The topologies and max. SLL comparison of the regular and space-tapered arrays for a beam scanned inside the sector are shown in Fig. 1 and Fig. 2, respectively (where iteration-0 corresponds to the regular array layout). Note that the SLL performance of the optimized array is maintained for varying scan angles within the sector [5].

We further assume that M = 64 element array is serving K = 4 randomly located simultaneous co-frequency users within a sector of ±45 deg. in user azimuth with a maximum range of $r_{\max}$. This scenario is visualized in Fig. 3. While serving a user, the side lobes of the beam generated by an array will cause interference (whose strength depends on the user distance) towards the others, as visualized in Fig. 4. This will reduce the SINR and thus, the throughput at the user ends.

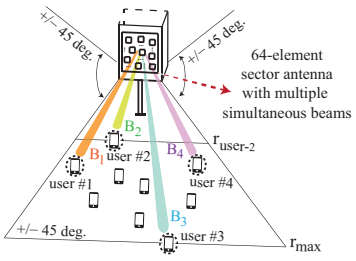

Fig. 3. A +/-45 degree sector antenna with 64 elements serving 4 users in the same time-frequency source block (side lobes are not shown for simplicity).

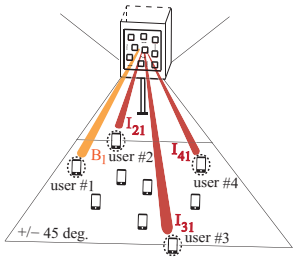

Fig. 4. Interference towards the other simultaneous, co-frequency users for beam #1.

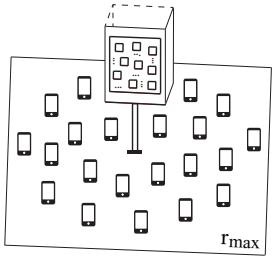

Fig. 5. Uniform user distribution in a cell around the base station.

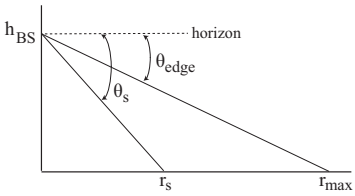

Fig. 6. Definition of the edge angle (θ_{edge}), scan angle in elevation (θ_s) and corresponding distances from the base station.

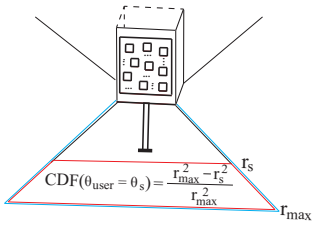

Fig. 7. Visualization of the area covered when θ_{user} is scanned from θ_{edge} to θ_s.

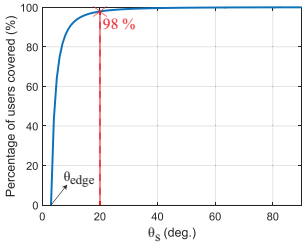

Fig. 8. Percentage of user coverage with respect to θ_s in a cell with uniformly distributed users over the area for h_{BS} = 10.5 m, $r_{\max}$ = 200 m.

The motivation of using space-tapered arrays is to reduce this interference by the help of the reduced SLL's in the case of CB, and approach to the performance of ZF which completely eliminates the inter-user interference.

The users are uniformly distributed in the cell area as shown in Fig. 5. The relation between the user elevation angle corresponding to the cell edge (θ_{edge}), base station height (h_{BS}), scan angle in elevation (θ_s) and corresponding range (r_s) is shown in Fig. 6. The area covered when the elevation angle is scanned from θ_{edge} to θ_s is computed as in Fig. 7 in terms of a cumulative density function (CDF). The result is plotted in Fig. 8 which shows that 98% of users are in the first 20 degrees below the horizon. Four random user positions are to be selected according to Fig. 8 in elevation and from a uniform distribution in ±45 degrees in azimuth. The assigned user positions at a time should be controlled in the MAC layer scheduling. One option is to select completely random positions, which is commonly applied in papers focusing

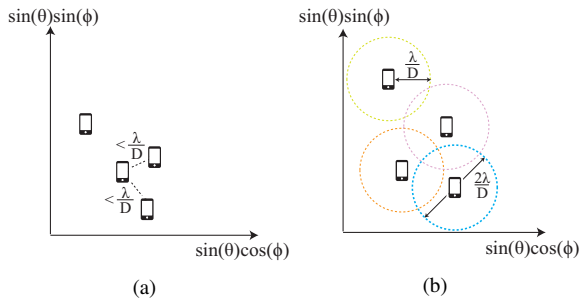

Fig. 9. Random scheduling of 4 concurrent co-frequency users among all the users in a sector, (a) interference-unaware, (b) interference-aware.

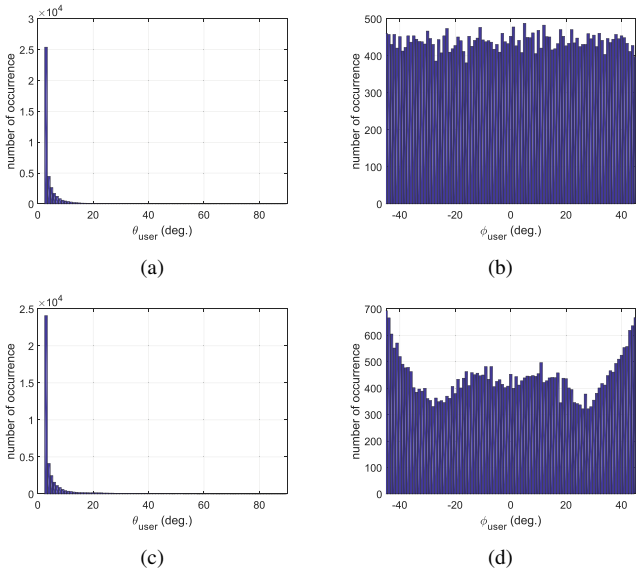

Fig. 10. Histogram of angular positions for 4 users and 10,000 random realizations, (a) interference-unaware, θ_{user}, (b) interference-unaware, ϕ_{user}, (c) interference-aware, θ_{user}, (d) interference-aware, ϕ_{user}.

only on the signal processing aspects. This approach will be referred as the interference-unaware scheduling in this paper (see Fig. 9(a)). A smarter approach is to consider the main beamwidth of the antenna in which no other co-channel users are allowed to enter. This will be called as the interference-aware approach since, when there are two users in the main beam of an array, either the interference between them will be very large (in the case of CB) or the user SNR's will be very low (in the case of ZF). In this work, we keep the minimum angular separation at λ/D radians as seen in Fig. 9(b) (which is approximately the half main beamwidth of the regular and space-tapered arrays) where D is the side length of the regular array. Histograms of the selected user positions for 10,000 random realizations for the two scheduling approaches are shown in Fig. 10, which are used to obtain the results given in Section III.

III. Numerical Results

The results of the described cell sector simulation are discussed in this section. Table I provides the simulation parameters and design values. The interference from adjacent sectors and cells is not considered. Each user is assumed to have a single omni-directional antenna. Mutual coupling is not taken into account and the embedded pattern of a patch element is assumed to be equal to $\sqrt{\cos\theta_{sc}}$, where θ_{sc} is the scan angle in spherical coordinates which is different from the user elevation angle, θ_s. Four different cases are investigated that differ in scheduling approach, errors in CSI estimation and quantization in antenna excitations. Three approaches are studied: regular array with CB, space-tapered array with CB and regular array with ZF. Space-tapered array with ZF performs very similar to the regular array with ZF since they both are able to null the interferences effectively and therefore, it is not included in the analyses.

TABLE I
LIST OF SECTOR SIMULATION PARAMETERS

Parameter definition	Symbol	Value
Center frequency (GHz)	f_c	28
Number of antennas	M	64
Number of simultaneous co-frequency users	$K^{(*)}$	4
Maximum cell radius (m)	$r_{\max}$	200
Angular width of a sector in azimuth (deg.)	Φ_{sector}	± 45
Base station height (m)	h_{BS}	10.5
Scan angle in elevation towards the cell edge (deg.)	θ_{edge}	3
Directivity of each antenna element at Tx (dB)	$D_{tx,el}$	8
Directivity of each user antenna at Rx (dB)	D_{rx}	0
Maximum average transmit power per user (dBm)	$P_{\max}{}^{(**)}$	26
Thermal noise (dBm)	P_{th}	-80
Number of random user location realizations	N_{sim}	10,000

(*) K can be increased while increasing the input power accordingly. In that case, INR in CB will increase, but proper ZF should still cancel all the interference.
(**) In this work, we apply adaptive transmit power control in order to equalize the power flux at the user ends. The users that are close to the base station require less transmit power to achieve similar power flux with the faraway users. Transmit power of the j-th user is given by; $P_j = P_{\max} \frac{(d^2_{user,j})}{\max(\boldsymbol{d}^2_{user})} \frac{\cos(\min(\boldsymbol{\theta}_{sc}))}{\cos(\theta_{sc,j})}$, where $\boldsymbol{d}_{user}$ is a vector consisting of the distances between the users and the base station.

A. Interference-unaware scheduling, perfect CSI, non-quantized excitations

Fig. 11 provides the results for interference-unaware scheduling with perfect CSI and non-quantized excitations in terms of the CDF of signal-to-noise ratio (SNR), interference-to-noise ratio (INR) and signal-to-interference-plus-noise ratio (SINR) at all users for all random realizations. It is seen that very low SNR's can be observed in ZF, while INR's can be quite large in CB. Both effects occur when the angular inter-spacing of the users are smaller than the main beamwidth of the base station antenna, which results in very low SINR's.

B. Interference-aware scheduling, perfect CSI, non-quantized excitations

In this case, the user scheduling approach is changed to guarantee a minimum angular separation among the users that

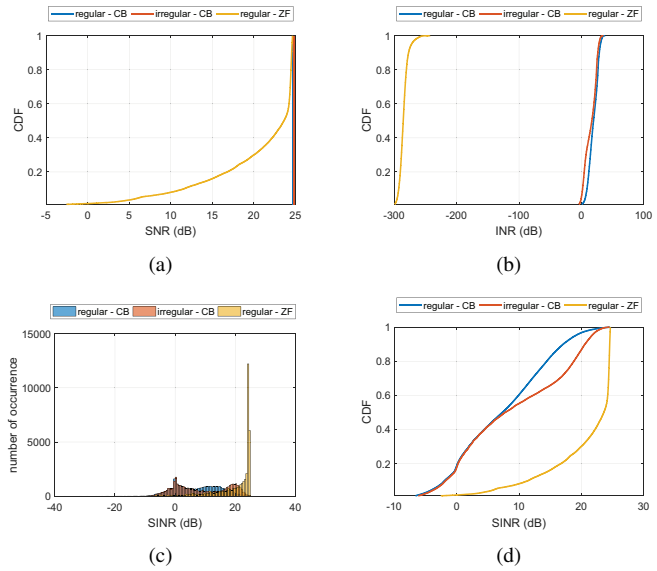

Fig. 11. Results of Case A: Interference-unaware scheduling, perfect CSI, non-quantized excitations, (a) CDF of SNR, (b) CDF of INR, (c) histogram of SINR, (d) CDF of SINR.

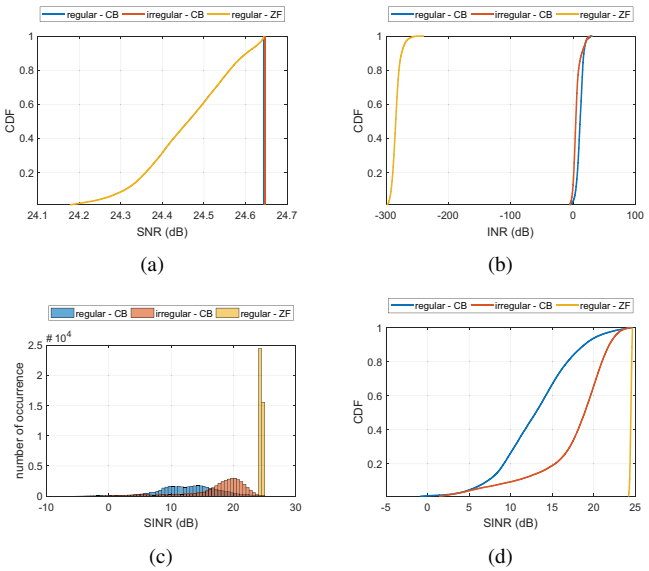

Fig. 12. Results of Case B: Interference-aware scheduling, perfect CSI, non-quantized excitations, (a) CDF of SNR, (b) CDF of INR, (c) histogram of SINR, (d) CDF of SINR.

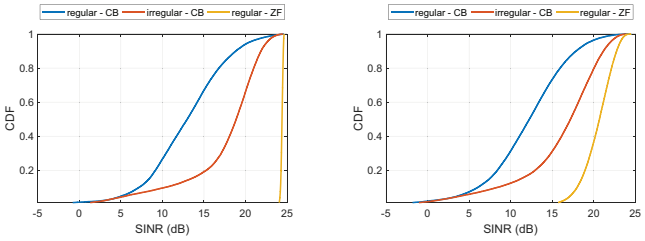

Fig. 13. SINR results of Case C: Interference-aware scheduling, imperfect CSI, non-quantized excitations, (a) max error of 0.001, (b) max error of 0.01.

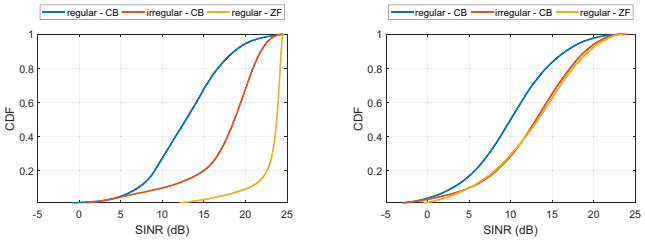

Fig. 14. SINR results of Case D: Interference-aware scheduling, perfect CSI, quantized excitations, (a) 0.5 dB amplitude step, 4-bit phase, (b) 0.5 dB amplitude step, 2-bit phase.

is larger than the half main beamwidth. The results are given in Fig. 12, which show significant improvement compared to the results in Fig. 11. It is seen that all the three approaches can achieve very good SNR, while the interference is nearly zero in ZF and maximum in CB with the regular array (which is expected due to the high SLL's seen in Fig. 2). Fig. 12(d) shows that the SINR in 90% of the cases is larger than 7.23 dB, 10.43 dB and 24.31 dB for the regular array with CB, space-tapered array with CB and regular array with ZF, respectively. Note that although it occurs rarely, the side lobes of faraway users in CB may create very large interference towards the closeby users. Therefore, it is preferable to treat the closeby

users with a separate sub-band and possibly a separate antenna, which is not discussed in this paper.

C. Interference-aware scheduling, imperfect CSI, non-quantized excitations

The effect of CSI errors on the results in Fig. 12 is studied here. The impurities in CSI is realized by adding normally distributed random complex numbers in every element of $\boldsymbol{H}$ within a certain maximum error range. Fig. 13 provides the CDF of SINR for two different maximum error values. It is seen that if the error is smaller than 0.001, the result in Fig. 12(d) is completely recovered. However, increasing the errors deteriorates the performance, as expected. Fig. 13(b) shows that for a maximum error of 0.01, the SINR in 90% of the cases is larger than 6.08 dB, 8.54 dB and 17.96 dB for the regular array with CB, space-tapered array with CB and regular array with ZF, respectively. This shows that CB is more robust to imperfect CSI (at relatively small errors) compared to ZF, which relies on placing perfect nulls at interferer positions.

D. Interference-aware scheduling, perfect CSI, quantized excitations

Effect of amplitude and phase quantization of the antenna weights on the user SINR performance is studied here by rounding the ideal weights to the practically available ones. Since CB does not apply amplitude tapering and ZF yields very small excitation amplitude ranges (only a few dB's), the main focus is on the phase shifters while keeping the amplitude steps at 0.5 dB. The results with 4-bit and 2-bit phase shifters are given in Fig. 14. It is seen that for 4-bit phase shifters, the results in Fig. 14(a) become similar to the ones in Fig. 13(b). However, Fig. 14(b) shows that for 2-bit phase shifters, the SINR in 90% of the cases is larger than only 3.12 dB, 5.14 dB and 5.15 dB for the regular array with CB, space-tapered array with CB and regular array with ZF, respectively. This shows that CB is more robust to phase quantization than ZF and that CB with space-tapering performs equally well as ZF statistically, when the number of phase bits is small.

IV. Conclusion

A comparative study on the statistical performance of conventional regular array layouts and space-tapered arrays with minimized SLL's has been performed in a LoS only propagation environment within an isolated cell sector. Mutual coupling has not been taken into account and each user has been equipped with a single omni-directional antenna.

The multi-user SDMA channel model has been formulated. A meaningful mm-wave link-budget analysis has also been incorporated into the model. Three different types of array layout and precoding technique combinations have been investigated, namely the regular array with CB, space-tapered array with CB and regular array with ZF. Four different simulation cases have been examined that differ in user scheduling approach, errors in CSI estimation and quantization in antenna excitations.

From the simulation results, the following main observations have been made.

1) A certain minimum angular spacing among the simultaneous co-frequency users has to be satisfied in user scheduling to guarantee high SNR values in zero-forcing and low interference levels in conjugate beamforming.
2) In interference-aware scheduling with homogeneous user distribution in a cell area, beam steering in elevation occurs very rarely and does not have a significant impact on the SINR in the statistical sense.
3) Space-tapered arrays with minimized SLL's statistically perform better than the regular arrays with uniform amplitudes in the case of CB.
4) ZF with regular (or irregular) arrays has the best statistical SINR performance in the interference-dominated scenarios under investigation. However, it is not robust to the errors in the estimated channel matrix or quantization in the excitation weights.
5) Despite of its computational simplicity, CB shows similar to ZF results in cases when either the propagation channel model is not known exactly or there are large quantization errors by beamforming. In any case, combination of CB with optimized arrays provides statistically sufficiently high SINR levels.

Acknowledgment

This research was conducted as part of the NWO-NXP Partnership Program on Advanced 5G Solutions within the project titled "Antenna Topologies and Front-end Configurations for Multiple Beam Generation". More information: www.nwo.nl.

References

[1] G. Gottardi, G. Oliveri, and A. Massa, "New antenna design concept for future generation wireless communication systems," in *Proc. 12th EuCAP*, London, UK, Apr. 2018.

[2] V. Degli-Esposti *et al.*, "Ray-tracing-based mm-wave beamforming assessment," *IEEE Access*, vol. 2, pp. 1314–1325, Nov. 2014.

[3] N. Amani *et al.*, "Network model of a 5G MIMO base station antenna in a downlink multi-user scenario," in *Proc. 12th EuCAP*, London, UK, Apr. 2018.

[4] Y. Aslan *et al.*, "Synthesis of multiple beam linear arrays with uniform amplitudes," in *Proc. 12th EuCAP*, London, UK, Apr. 2018.

[5] Y. Aslan *et al.*, "Multiple beam synthesis of passively cooled 5G planar arrays using convex optimization," *IEEE Trans. Antennas Propag.*, submitted for publication.

[6] H. Q. Ngo, Massive MIMO: Fundamentals and System Designs. Nottingham, U.K: Linköping Univ. Electronic Press, 2015.

[7] X. Ge *et al.*, "Multi-user massive MIMO communication systems based on irregular antenna arrays," *IEEE Trans. Wireless Commun.*, vol. 15, no. 8, pp. 5287–5301, Aug. 2016.

[8] C. Bencivenni *et al.*, "Effects of regular and aperiodic array layout in multi-user MIMO applications," *Proc. IEEE USNC/URSI NRSM*, San Diego, CA, USA, Jul. 2017.

[9] B. Yang *et al.*, "Digital beamforming-based massive MIMO transceiver for 5G millimeter-wave communications," *IEEE Trans. Microw. Theory Tech.*, vol. 66, no. 7, pp. 3403–3418, Jul. 2018.

[10] T. Kim *et al.*, "Tens of Gbps support with mmwave beamforming systems for next generation communication," in *IEEE GLOBECOM'13*, Dec. 2013, pp. 3790–3795.

[11] W. Roh *et al.*, "Millimeter-wave beamforming as an enabling technology for 5G cellular communications: Theoretical feasibility and prototype results," *IEEE Commun. Magn.*, vol. 52, no. 2, pp. 106–113, Feb. 2014.

[12] A. A. Glazunov, "Impact of deficient array antenna elements on downlink massive MIMO performance in RIMP and random-LoS channels," in *Proc. 12th EuCAP*, London, UK, Apr. 2018.

[13] C. S. Park *et al.*, "Complexity reduced zero-forcing beamforming in massive MIMO systems," in *Proc. IEEE ITA*, San Diego, US, Feb. 2014.